Exposure Image Fusion of Enhancing Detail Visibility Based on Contrast Adjustment

GUO-CHENG YANG[1,2,3] MEI-LING LI[4] LEI-TING CHEN[1,3] HANG QIU[1,3]
[1] School of Computer Science and Engineering, University of Electronic Science and Technology of China, Chengdu, CHINA
[2] Department of Biomedical Engineering, Sichuan Medical University, Luzhou, CHINA
[3] Provincial Key Laboratory of Digital Meida, Chengdu, CHINA
[4] School of Life Science and Technology, University of Electronic Science and Technology of China, Chengdu, CHINA
gchyangli@163.com

Abstract: -To extract fine details from input bracketed images and preserve them in the final image, a novel exposure fusion method based on the nonsubsampled contourlet transform (NSCT) is presented in this paper，in which unique visual weight map is used for the detail extraction and an improved weight measurement is developed to remove the motion objects in dynamic scenes. Furthermore, a fast algorithm for contrast enhancement is applied to adjust the contrast of decomposition subbands and gain control is also introduced to modify the visibility of the blended subbands at different scales. Finally, the resulting image with more visible details is reconstructed by the inverse NSCT. Experimental results demonstrate that the proposed method can preserve fine details and produce sharper images, especially in enhancing detail visibility in the dark areas.

Key-Words: - Exposure fusion, NSCT, Weight map, Contrast enhancement, Gain control

1 Introduction

High dynamic range (HDR) image has a much larger scope range than low dynamic range (LDR) image. However, most display devices only have limited dynamic range. In essence, a single image captured by standard digital camera only contains a portion of feature information in real-world scenarios, so the pictures taken by a conventional camera often result in the loss of detail information. Although some professional HDR devices can be exploited to capture the real scene information, but these professional devices are very expensive and not appropriate for most users. On the other hand, users may apply HDR imaging techniques to reconstruct a HDR image from a set of LDR images [1, 2], and then use tone mapping techniques to derive a LDR image that can be visualized on standard devices in [3-6] . However, tone mapping is time consuming and not efficient for requiring camera parameters to calculate the radiometric response function. Comparing with these schemes above, exposure fusion is a good way to implement the rendering of an HDR image on a conventional LDR display device, which can recover the full dynamic range of a natural scene without generating of an intermediate HDR image. Thus application of this technique can extract abundant information from the source images and preserve them for the fused result.

So far, various techniques have been developed for exposure fusion so that the information of the source images can be fully visualized. Mulscale decomposition image fusion based has been recognized as the effective work and achieved rapid development in the past decades. Many mulscale transform tools have been developed and applied to image fusion. For example, the pyramid decomposition [7-9], discrete wavelet transform (DWT) [10], anisotropic diffusion (ASD) [11], contourlet (CT) [11, 12] and nonsubsampled contourlet transform (NSCT) [13], and so on. Compared with other multiscale transforms, NSCT is a more prominent tool for image decomposition. Because of its multiscale, multidirection and full shift invariance, it can efficiently capture higher dimensional singularities and avoid pseudo-Gibbs phenomena that presents in the contourlet transform. Specifically, the impact of misregistration on the fused results is also reduced effectively [14]. These properties are more suitable for image fusion.

Usually, the underexposed or overexposed images usually show the low resolution in some regions even the whole areas. Whereas color balance and contrast enhancement have the strong impact on visual effect. Thus, before image fusion, performing contrast enhancement for the input sequence is can efficiently improve image quality. Inspired by the method in the literature [15], we implement the contrast adjustment of subband images by solving a Poisson equation, with two different variants. This new tool is fast and efficient, requiring no manual selection. Another advantage is to brighten up areas of poor contrast but not at the expense of saturating areas of good contrast.

In this paper, we propose a novel exposure fusion scheme based on NSCT, which employs different weight measurements to compute weight maps of input images in the static and dynamic scenes, respectively. This method not only extracts fine detail information of the original images, but also provides the artifact-free reproduction for the dynamic scenes. Moreover, to increase the local contrast in the dark areas and improve the brightness of the final image, gain control is also introduced to adjust the brightness of the blended subbands.

The rest of this paper is organized as follows. In Section 2, related researches are reviewed. In Section 3, we first give a brief introduction of the proposed workflow and NSCT, and then detailedly describe the implement process of the proposed fusion algorithm. Experimental results and analysis are illustrated in Section 4. Lastly, conclusions are given in Section 5.

2 Related Researches

Exposure fusion, as a subarea of image fusion approaches, is a recently developed technique for extracting more details from a set of exposure images. During the past decades, numerous exposure fusion approaches have been proposed to synthesize a high quality image, aiming to maximize the information contents of the final image. For example, Goshtasby et al. partitioned source images into uniform blocks, and selected those blocks containing the most information to synthetize an image in [16]. Mertens et al. fused the bracketed images into a high quality image using Gaussian and Laplacian pyramid decomposition in [17]. Raman and Chaudhuri used edge-preserving bilateral filter for fusing exposure images, in which the appropriate matting function was generated for automatic process in [18] More recently, a probabilistic model that preserves the luminance levels and a quadratic optimization based method were respectively proposed to generate the final image with more details in [19, 20].

Most existing exposure fusion techniques are only suitable for static scene [20, 21]. However, images captured by natural scenes usually contain the motion objects, so these methods mentioned above may produce serious distortions in dynamic scenes, resulting in annoying ghost artifacts in the resultant image. Many solutions that adapt to dynamic scenes have been presented to eliminate the adverse impacts caused by motion objects. For instance, Gallo et al. produced an artifact-free HDR image by averaging the radiance estimates of all patches which were consistent with a reference image in [22]. Shen et al. presented a detail-preserving exposure fusion method using subband architecture in [23], which generated a ghost-free product by mask images. Although these methods produced an image without ghost artifacts, the fusion process needed to preselect a reference image or mark the moving objects by manual intervention. In addition, in [24, 25], the methods based on gradient information and median filter were used to merge a set of images from dynamic scenes into a ghost-free image. However, the fusion image produced by these methods usually suffers from the loss of detail information. Unlike the traditional exposure fusion approaches, the proposed scheme not only extracts fine details in the source images, but also effectively removes ghost artifacts.

3 Proposed Algorithm

Fig. 1 shows the schematic diagram of the proposed exposure fusion method. First, each source image is decomposed into a low-pass image and a series of high frequency subimages using NSCT, and simultaneously weight map of each input image is computed and used for extracting detail information from the source images. Then a fast algorithm for contrast enhancement with two simple variants is used to tune all decomposition subband coefficients, which helps to improve color balance and contrast of decomposition subbands while conserving good global appearance. Further, gain control maps are introduced to rectify the brightness of all blended subimages, the purpose of which is to augment the visibility of details at various scales. Finally, the resultant image with more visible details is reconstructed by the inverse NSCT. For the simplicity of illustration, the image processing workflow only describes the fusion process using two input images $I(A)$and $I(B)$ as a special case. Obviously, the proposed scheme can be easily extended to fuse multiple images

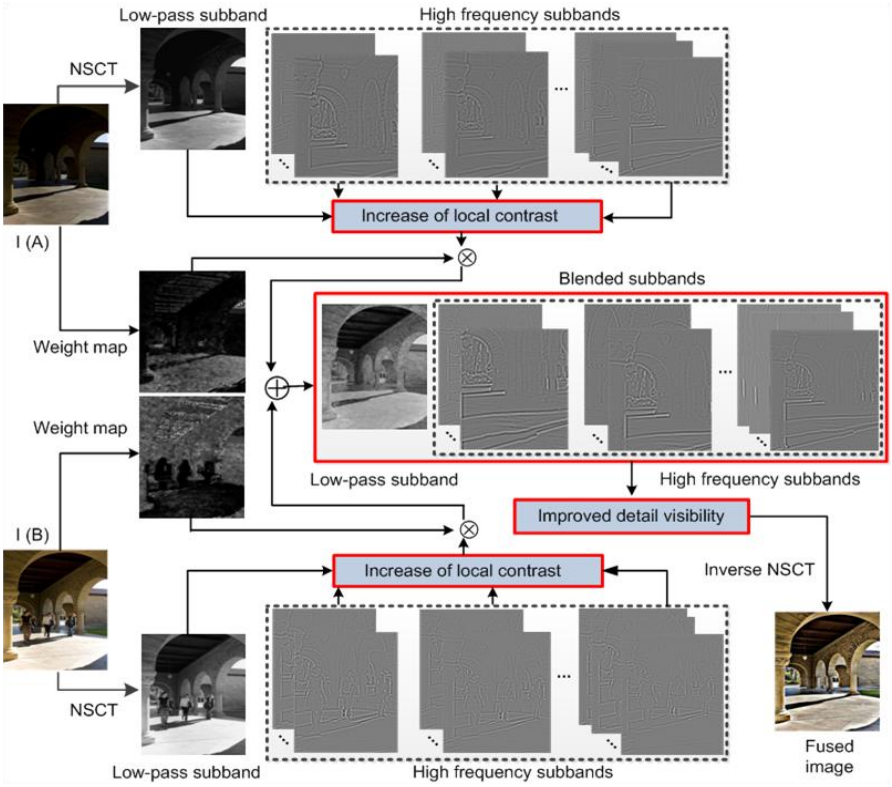

Fig. 1 The general framework of the proposed method

3.1 NSCT based image analysis

NSCT, as a shift invariant version of contourlet, is a fully shift-invariant, multiscale, and multidirection expansion that has a fast implementation [13] and the whole process is divided into two phases, namely nonsubsampled pyramid (NSP) and nonsubsampled directional filter bank (NSDFB), which is achieved by using two-channel non-subsampled 2D filter banks. The former performs multiscale decomposition and the later provides direction information. The NSP divides image into a low frequency subband and a high frequency subband at each decomposition level. If the decomposition level is k, NSP can generate $k+1$ subimages, which consists of one low-pass image and k high frequency images. The subsequent NSDFB decomposes all high frequency subbands from NSP. Assume that l_j denotes the direction numbers of the NSDFB at the j th scale. The number of the directional subbands produced at the corresponding scale is 2^{l_j}, whose sizes are all the same as the source image. After the low frequency component is iteratively decomposed in the same way, an image is finally decomposed into one low frequency subimage and a series of high frequency subimages. When the NSCT is introduced to the image fusion, its perfect properties will benefit designing fusion rules

3.2 Detail Enhancement

To increase the local contrast and enhance the important details in the dark and bright areas, the exponential transfer function, as one of basic image enhancement functions, is applied to perform multiscale contrast stretching so as to tune subband coefficients at each scale. The relationship between the enhanced subband coefficients and the original subband coefficients at the jth scale with the dth direction is derived as

$$C'^{I}_{j,d}(x,y) = \left(C^{I}_{j,d}(x,y)\right)^{(1-m_d)} \quad (1)$$

where m_d is a positive and scale-related parameter (its value is set to 0.03), which can control the degree of enhancement.

3.3 Construction of Visual Weight Map

Weight map objectively reveals the visual importance of each pixel of the original images. In principle, these pixels which are the lower brightness, saturation should be assigned smaller values, and these pixels with abundant detail information should be given greater values. In this study, a unique image quality measurement is exploited to compute weight which utilizes the characteristics that Human Visual System is sensitive to the contrast, intensity and color difference of image. The visual weigh maps are

calculated by three key factors, namely visibility, saturation and well-exposedness. Considering the practicability and robustness of the algorithm, weight extraction in static scenes and dynamic scenes is respectively defined as

$$W_{S_i} = V_i(x,y) \times S_i(x,y) \times E_i(x,y) \quad (2)$$

$$W_{d_i} = C_i(x,y) \times S_i(x,y) \times E_i(x,y) \quad (3)$$

where W_{S_i}, W_{d_i} represents weight of the pixel of the location (x,y) for the ith exposure image in static or dynamic scenes. $V_i(x,y)$, $C_i(x,y)$ $S_i(x,y)$, $E_i(x,y)$denotes the visibility, consistency, saturation, exposure respectively.

3.3.1 Visibility Measurement

Usually, exposure fusion method guided by visibility is beneficial to produce a result with fine details. Mathematically, the visibility is calculated by gradient magnitude of input image, which tends to assign larger weight for these pixels such as edges or corners. The measurement is defined as

$$I_x^i = I^i(x,y) \otimes \frac{\partial}{\partial_x} g(x,y{:}\,\sigma_d) \quad (4)$$

$$I_y^i = I^i(x,y) \otimes \frac{\partial}{\partial_y} g(x,y{:}\,\sigma_d) \quad (5)$$

$$V^i(x,y) = \sqrt{\left|I_x^i(x,y)\right|^2 + \left|I_y^i(x,y)\right|^2} \quad (6)$$

where $I_x^i(x,y)$ and $I_y^i(x,y)$ are the partial derivatives of the x and y directions in the source images, respectively. σ_d is the standard deviation.

3.3.2 Consistency Measurement

According to the fact that the gradient direction will have significant changes for some areas where there exist the moving objects among different images [24], we apply gradient direction change to detect the inconsistency information caused by the motion targets and further remove ghost artifacts. The consistency is measured in a window based manner and the azimuth angle of the ith input image is defined as

$$\theta^i(x,y) = arctan\frac{I_y^i(x,\ y)}{I_x^i(x,y)} \quad (7)$$

The gradient direction change between ith image and jth image is calculated from Eq. (8). Further, we get cumulative gradient direction changes, namely $C^i(x,y)$, as is defined as Eq. (9). Unlike the method by Zhang et al. [24], the proposed algorithm strengthens the sensitivity of consistency using a gamma function. Apparently, the larger gradient direction change will give rise to the smaller $C^i(x,y)$, which indicates that the pixels contained within the motion objects have very small weights. Here, the index γ is set to 3.

$$d_{ij}(x,y) = \frac{\sum_{-l}^{l}\left|\theta^i(x+k,y+k) - \theta^j(x+k,y+k)\right|}{(2l+1)^2} \quad (8)$$

$$C^i(x,y) = \left(\sum_{j=1}^{N} exp\left(\frac{-d_{ij}(x,y)^2}{2\sigma_s^2}\right) - 1\right)^{\gamma} \quad (9)$$

3.3.3 Saturation Measurement

The depth of color saturation of an image has great influence on visual perception and the saturated color make it look vivid. For some underexposed or overexposed regions, the color will become faded. Similar to the method in [17], in this paper, the saturation $S_i(x,y)$ is represented as Eq. (10). Here, U is the mean value of R, G, B (red, green and blue color channel).

$$S_i(x,y) = \sqrt{(R-U)^2 + (G-U)^2 + (B-U)^2/3} \quad (10)$$

3.3.4 Exposure Measurement

Just looking at the visual effect, the overexposed regions show nearly white (intensity values of pixels are almost 1), whereas the underexposed regions display nearly black (intensity values of pixels are almost equal to 0). To abandon these pixels which are underexposed or overexposed areas and record those pixels with better brightness values, Exposure E_i is calculated as

$$E_i(x,y) = e^{-\frac{(R-0.5)^2}{2\theta^2}} \times e^{-\frac{(G-0.5)^2}{2\theta^2}} \times e^{-\frac{(B-0.5)^2}{2\theta^2}} \quad (11)$$

3.4 Contrast adjustment

Image contrast enhancement is an important issue in image processing, it will balacce global and local contrast changes and reduce chroma distortions. A lot of contrast enhancement techniques have been used for improving the contrast of an image [26, 27]. However, there is no universal method for all applications, mostly because the kind of correction depends on the scene. In this paper, the main idea of the contrast adjustment is to modify the gradient vector field and to solve the corresponding Poisson equation with two variants in [28], the first of which adjusts the contrast by increasing the gradient in the dark regions of the image and the other one enhances

all small gradients in the image. In view of uneven exposure situation for the input images, we utilize the selective contrast adjustment on different kinds of exposure images. When the selective regions are on the dark regions of the image Ω, namely "Enhanced dark", we will obtain the contrast with good results using a simple function. The region Ω and the guidance vector field are defined as

$$\Omega = \{x \in R: f(x) \leq T\} \tag{12}$$

$$V = \begin{cases} a\nabla f & in\ \Omega_d \\ \nabla f & otherwise \end{cases} \tag{13}$$

In the implementation, the parameter T and a, as default values, are set to 50 and 2.5. On the other hand, in order to modify the gradient over the whole image and not just on dark regions, namely "Enhanced global". Usually, the norm of the vector field becomes a power of the norm of the gradient and a concave power is adapted to enhance small image details, whereas a convex power may be adapted to overexposed images. Thus we may use a concave power function to reduce the large gradients and increase the small ones. The guidance vector field is computed as

$$V = |\nabla f|^{\alpha-1}\nabla f \tag{14}$$

where the value for α is 0.8, by default.

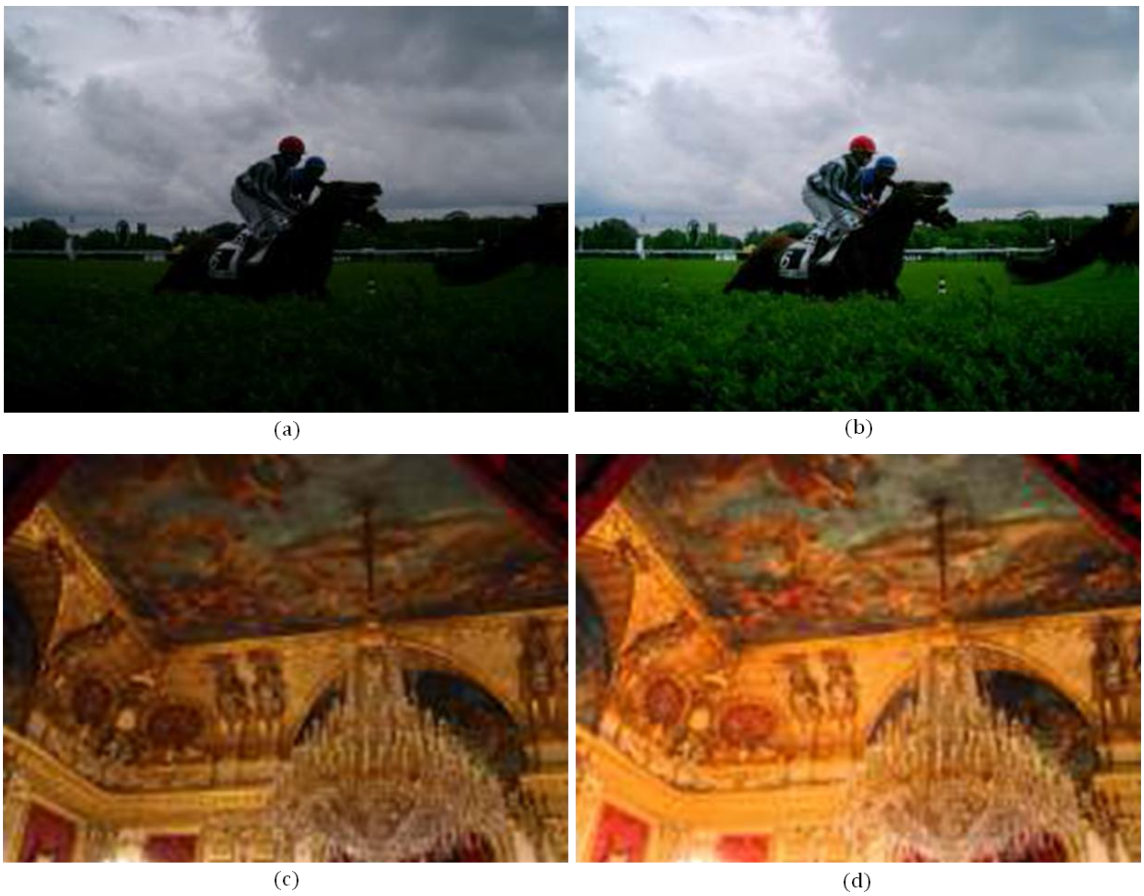

Fig. 2 Comparison between the original image and the result obtained by the contrast adjustment in [15]. (a) and (c) Original images. (b) and (d) The results by the "Enhanced dark" and "Enhanced global" with default parameters, respectively.

Fig. 2 illustrates the comparison between the original images and the results obtained by the contrast adjustment. As shown in Fig. 2, though the adjustment of contrast, the visual effects of two original images achieve the significant improvement, but do not produce artifacts. More important, perceptually black objects still remain black.

3.5 Fusion Process

In order to gain the visually consistent fusion result, we first normalize and smooth K weight maps above by a Gaussian kernel function, the corresponding weighted average is represented as $\overline{W_k}(x,y)$. Then the fused subband coefficients $C_k^F(x,y)$ is obtained from Eq. (15). Thereinto, $C_k^i(x,y)$ denotes the ith decomposition subband coefficients of the kth image.

$$C_k^F(x,y) = \sum_{i=1}^{N} \overline{W_k}(x,y) \times C_k^i(x,y) \quad (15)$$

3.6 Improvement of Detail Visibility

Gain control can effectively improve the sharpness of decomposition subbands, resulting in a detail-enhanced fused image, which has been successfully applied in [29, 30]. The procedure of constructing gain control map is as follows. First, an activity map can be expressed as Eq. (16). Then, the aggregated activity map $A_i(x,y)$ and gain map $G_i^{ag}(x,y)$ can be derived from Eq. (17) and (18). Lastly, the blended subband coefficients are modified using Eq. (16).

$$A_i(x,y) = g(\sigma) \otimes \left|C_i^F(x,y)\right| \quad (16)$$

$$A_{ag}(x,y) = \sum_{i=1}^{k} A_i(x,y) \quad (17)$$

$$G_i^{ag}(x,y) = m_i \left[\frac{\varepsilon + A_{ag}(x,y)}{\delta}\right]^{(\lambda-1)} \quad (18)$$

$$C_i^{F'}(x,y) = G_i^{ag}(x,y) \times C_i^F(x,y) \quad (19)$$

where, λ is a weight factor (set 0.8), ε is a small parameter that prevents the noise from blowing up, α is a constant related to spatial frequency. The parameter m_i is used to control the extent of frequency, and δ is a gain control stability level.

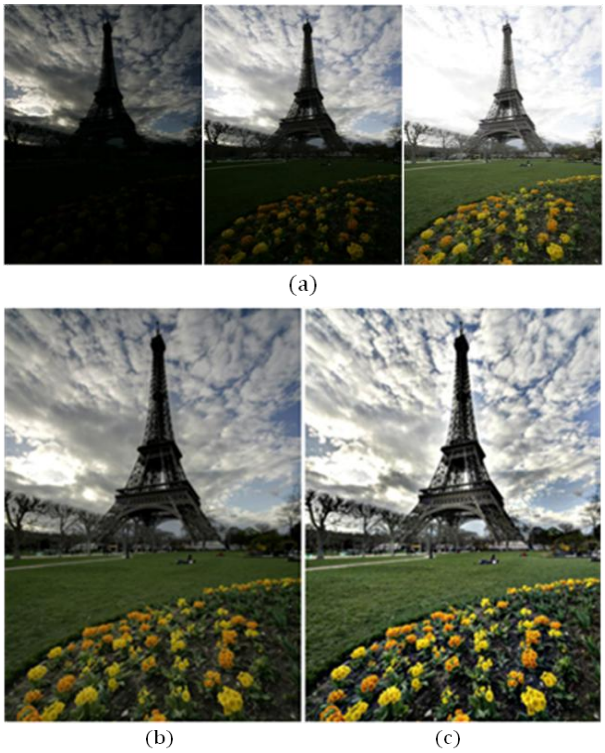

Fig.3 Comparison of the fused results without gain map and with gain map. (a) Input sequence. (b) Result by Mertens et al. [17]. (c) Our result (with gain control).

Fig. 3 shows the visual effect by using gain control. While for all the subbands are modified by the gain control maps, this technique does well in both preserving details and enhancing the brightness of the final image (see Fig. 3(c)).

4 Experimental Results and Analysis

Experiments are performed on six different exposure image sequences, four sets of which are taken in static scenes and the rest are from dynamic scenes. The fusion results are respectively compared with other existing exposure fusion approaches. Additionally, four objective image fusion quality metrics, namely average gradient (AG), information entropy (IE), uniform intensity distribution (UID) and gradient based index ($Q^{ab/f}$) are employed to assess the fusion performance of different results. Conceptually, AG reflects the clarity of an image, which measures the spatial resolution of the fused image [31]. IE indicates the amount of information including in an image [32], the higher value of which shows the fused image contains more information contents than the original images. UID is used for the description of uniform intensity and color distribution [33]. The higher UID shows that the final image attains better effect in term of brightness, uniformity and color. Moreover, the fusion quality index $Q^{ab/f}$ measures the amount of salient information transferred to the fused image, which quantifies the difference between the final image and the source images [34]. Thus, according to the implication of metrics above, the greater value shows the fusion performance is better.

4.1 Fusion of Images with Static Scenes

Fig. 4 provides a test of exposure fusion and our result is compared with the results produced by Li et al. [25] and Mertens et al. [17]. Obviously, all fusion results exhibit good colorfulness and brightness. However, see these regions where the red arrows are pointing in Fig. 4(a), (b) and (c) carefully, the proposed method obtains the best visual effect in terms of clarity, texture and detail visibility. In Fig. 5, another experiment is carried out, which gives the comparison of fusion performance between the proposed method and the classical method in [17]. As shown in the closeup views of Fig. 5(c) and (d), whether the texture details of the rock on the coast or the sharpness of the plants on the bank, the proposed method achieves better visual perception. Especially in the dark areas, the texture details are more apparent. Fig. 6 shows two other exposure fusion examples in static scenes including “Door” and “Igoo”, in which

our result is also compared with the final image in the recent method [35]. As shown in Fig. 6(b)-(f), we hardly discern the details of region marked by the red arrow in Fig. 6(c). Despite the results of Fig. 6(b) and Fig. 6(d) have some improvement, for these regions that are highlighted by the red arrows, their results are dim and blurred. Relatively, the final result (see Fig. 6(e)) of the scheme in [35] has a good contrast and clear texture, but the brightness of the marked regions is still low. In contrast, the proposed method not only well preserves detail information in bright regions but also enhances the brightness in the dark regions. The contrast and color adjustment also obtain better effect.

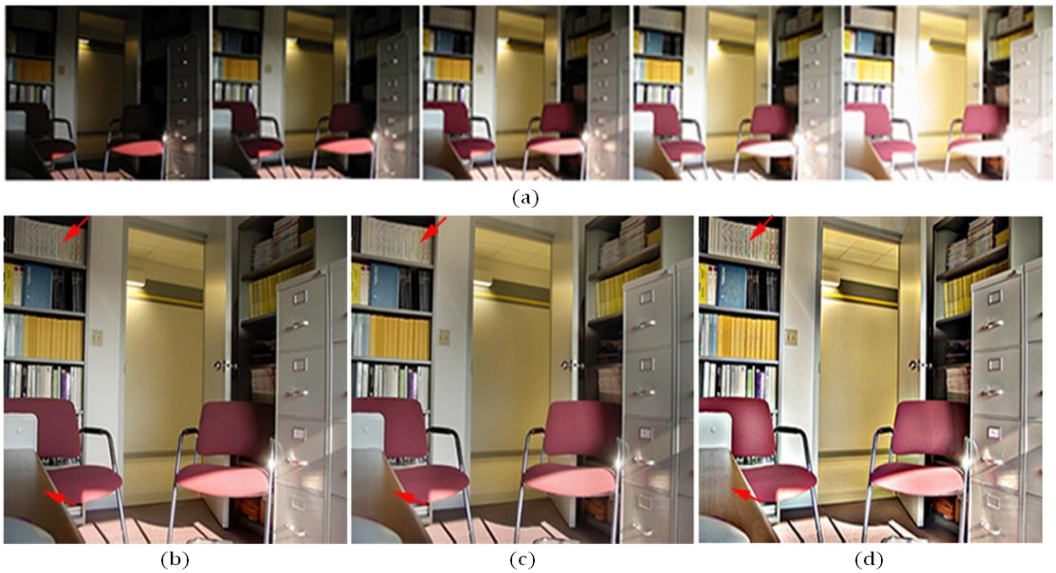

Fig.4 Comparison of test results by different approaches. (a) Input sequence. (b) Result by Li et al. [25]. (c) Result by Mertens et al. [17]. (d) Our result.

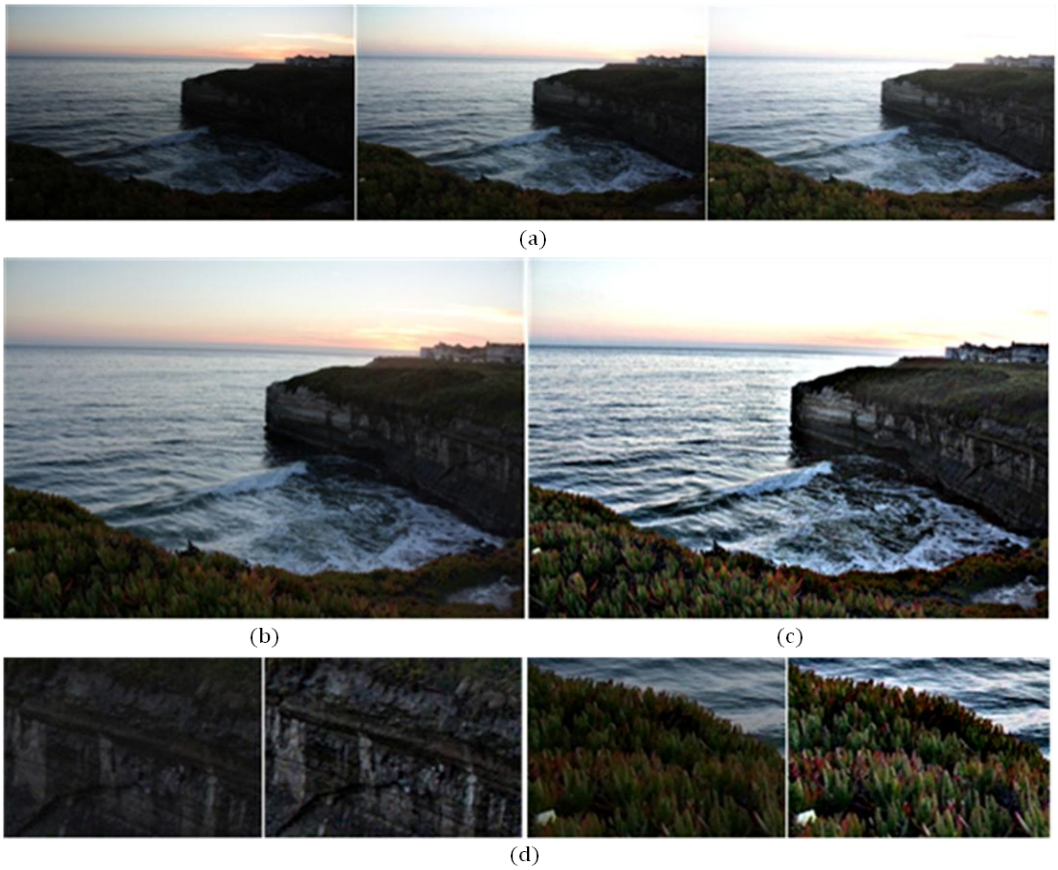

Fig.5 Comparison of test results by our scheme with the representative fusion method. (a) Input sequence. (b) Result by Mertens et al.[17]. (c) Our result. (d) Comparison of two close-up views (corresponding to rock on the coast and plants on the bank, and our results locate on the right side).

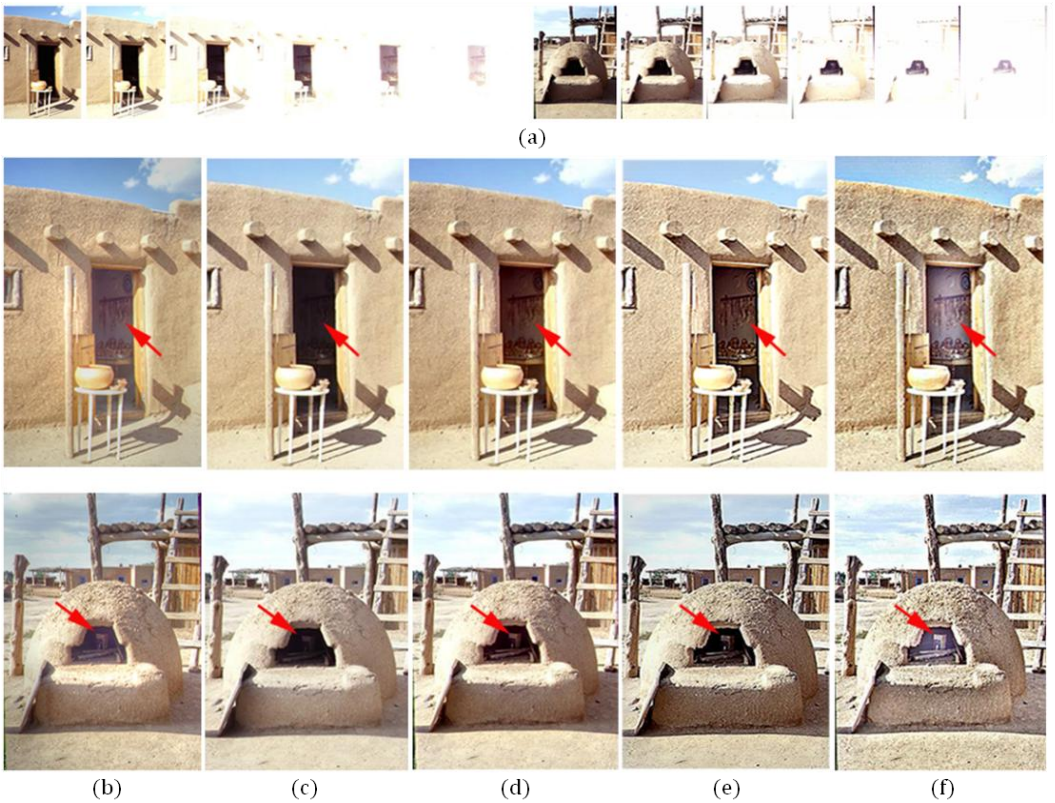

Fig. 6 Comparison of test results by different exposure fusion methods. (a) Input sequence. (b) Result by Fattal et al. [30]. (c) Result by Li et al.[25]. (d) Result by Mertens et al. [17]. (e) Result by Singh et al.[35]. (f) Our result. Two input sequences are are called "Door" and "Igloo", respectively.

4.2 Fusion of Images with Dynamic Scenes

Fig. 7 shows an example of verifying effectiveness of the proposed method in dynamic scenes, the scenes of which are several pedestrians in an arch corridor. Although the fusion scheme in [22] has de-ghosting function, it introduces serious blocking artifacts (see Fig. 7(b)). Again, it is low visibility and natural contrast for the ceiling areas (the top region labeled by the red arrows). Intuitively, both the proposed method and the scheme in [25] not only effectively remove ghost artifacts, but also well improve the sharpness, brightness and colorfulness of the final image. However, it is easy to see the difference between them from Fig. 7(e), which is respectively the histogram distribution of Fig. 7(c) and (d), the peaks of the histogram produced by our algorithm are more flattened and smooth, which demonstrates that it obtains the fused image with the higher clarity and contrast. In addition, by comparison of the zoom regions (as shown in Fig. 7(f)), where are the pillar bottom and floor of the building (the regions labeled by the red boxes in Fig. 7(b)), our method obviously produces the best result. As another testing example of exposure image fusion in dynamic scenes, input sequence of Fig. 8 shows a dynamic scene with several persons walking in the park. Obviously, the proposed method and the algorithm in [24] can thoroughly eliminate the negative effects caused by the motion objects and obtain a high quality image without ghosting artifacts. However, there is the case that our algorithm sometimes excessively enhances the brightness of some regions when most of the input images are overexposed images, resulting in the blocking effects at the edges of objects. Thus, for the proposed scheme, there is still work for improvement.

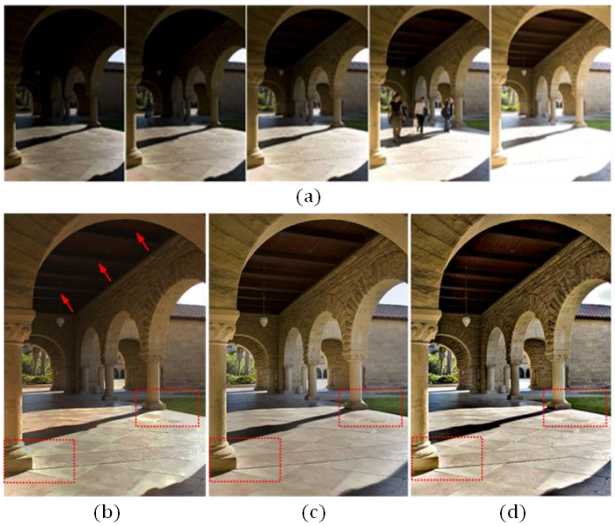

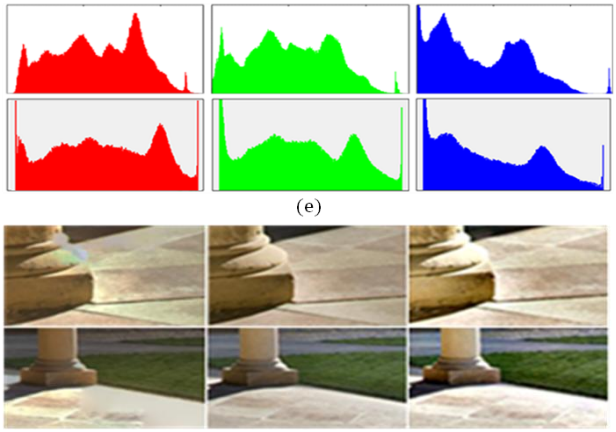

(e)

(f)

Fig. 7 Comparison of three exposure fusion schemes in dynamic scenes. (a) Input sequence. (b) Result by Gallo et al.[22]. (c) Result by Li et al. [25]. (d) Our result. (e) Histogram distribution of each R, G, B color-single-channel of (c) and (d). The first and second rows are the histogram distributions of three color channels in (c) and (d), respectively. (f) Close-up views of (b), (c). (d), in left-to-right order. From top to bottom, the zoom regions correspond to the pillar bottom and floor, respectively.

4.3 Objective Fusion Quality Evaluation

To verify the superiority of the proposed scheme, four objective image fusion quality metrics are employed to test the effectiveness and feasibility of our method. They evaluate the fusion performance from different aspects such as the clarity, visibility and containing the amount of information each other, Table 1 and Table 2 give the values of several indicators generated by different methods in static and dynamic scenes, respectively. As can be seen from two tables, the proposed method obtains the largest value for four quality evaluation indexes, which demonstrates that the proposed method provides a better performance in terms of the larger values for all tests. These results are consistent with subjective visual perception. It is also confirmed that, whether in static scenes or dynamic scenes, the proposed fusion method based on visual weight map and gain control can capture abundant information of the original images into the fused image.

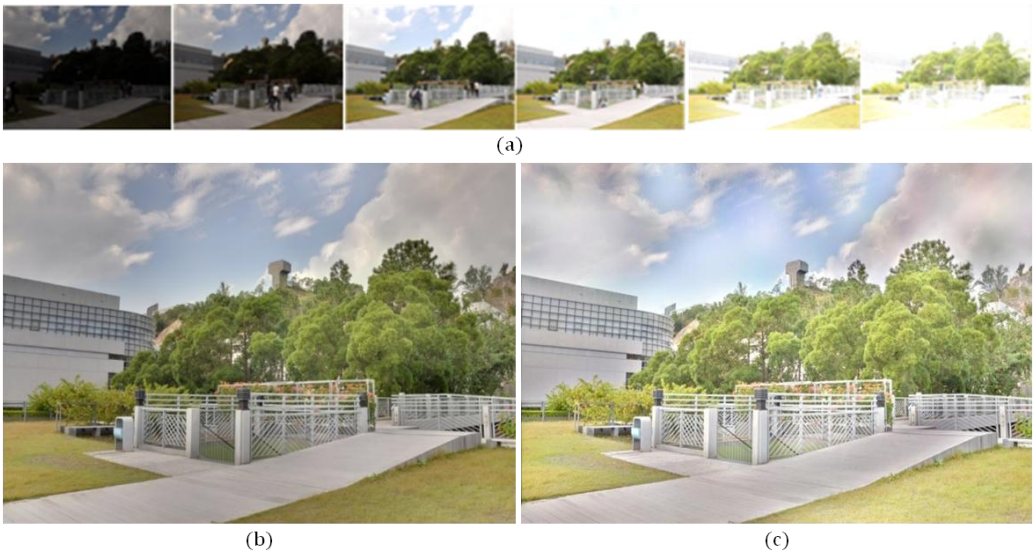

(a)

(b) (c)

Fig. 8 Comparison of two exposure fusion schemes in dynamic scenes. (a) Input sequence. (b). Result by Zhang et al. [24]. (c) Our result.

Table 1. Quantitative comparison of different exposure fusion methods in static scenes

Image	Index	Methods				
		Mertens et al.	Li et al.	Fattal et al.	Singh et al	Proposed
Door	AG	7.88	6.88	6.40	13.31	10.22
	IE	13.51	13.04	14.23	14.20	15.01
	UID	0.92	0.88	0.75	0.92	0.93
	$Q^{ab/f}$	0.61	0.59	0.51	0.64	0.68
Igloo	AG	10.40	8.31	8.96	9.52	12.05
	IE	13.57	13.01	14.61	13.42	15.56
	UID	0.92	0.91	0.88	0.89	0.92
	$Q^{ab/f}$	0.62	0.61	0.58	0.65	0.67

Table 2. Quantitative comparison of different exposure fusion methods in dynamic scenes

Fig. 7	Methods			Fig. 8	Methods	
Indexes	Li et al.	Gallo et al.	Proposed	Indexes	Zhang et al.	Proposed
AG	5.04	4.44	6.95	AG	4.94	6.33
EN	14.05	13.51	16.44	EN	14.31	15.07
UID	0.93	0.92	0.97	UID	0.86	0.89
$Q^{ab/f}$	0.51	0.51	0.58	$Q^{ab/f}$	0.50	0.59

5 Conclusions

We develop a novel multiple exposure fusion approach, which well extracts salient features of the original images using visual weight maps and increases the visibility of details by gain control. Moreover, utilizing of different image quality measurements, such as the visibility, saturation, well-exposedness and consistency, makes the algorithm applicable to both static scenes and dynamic scenes. Experimental results demonstrate the validity of the method, especially for the case that the interested regions are in low brightness. It is noted that the proposed scheme has the limitation of over-enhancement at the edges of objects when most of input images are overexposed. Ongoing research will optimize the fusion performance of the algorithm by introducing the theory of adaptive system.

Acknowledgements:

The authors would like to thank all the anonymous reviewers and editors for their instructive comments and suggestions on an earlier version of this paper, which significantly contributed to improving the quality of this paper. This work is supported by the Sheng-Bu Industry-Academia-Research joint project of Education Ministry and Science & Technology Ministry of Guangdong province (NO: 2012A090300001).

References:

[1] m. granados, b. ajdin, m. wand, and c. theobalt, "optimal hdr reconstruction with linear digital cameras." pp. 215 - 222.

[2] P. E. Debevec, and J. Malik, "Recovering High Dynamic Range Radiance Maps from Photographs," *Siggraph*, pp. 369-378, 1997.

[3] E. Reinhard, W. Heidrich, P. Debevec, S. Pattanaik, G. Ward, and K. Myszkowski, *High dynamic range imaging: acquisition, display, and image-based lighting*: Morgan Kaufmann, 2010.

[4] Z. Farbman, R. Fattal, D. Lischinski, and R. Szeliski, "Edge-preserving decompositions for multi-scale tone and detail manipulation." p. 67.

[5] F. Durand, and J. Dorsey, "Fast bilateral filtering for the display of high-dynamic-range images." pp. 257-266.

[6] S. Q, J. J, and B. MS, "Globally optimized linear windowed tone mapping," *IEEE transactions on visualization and computer graphics*, vol. 16, 2010.

[7] P. J. Burt, and E. H. Adelson, "The Laplacian pyramid as a compact image code," *Communications, IEEE Transactions on*, vol. 31, no. 4, pp. 532-540, 1983.

[8] Z. Liu, K. Tsukadab, K. Hanasakib, and Y. K. H. P. Daic, "Image fusion by using steerable pyramid," *Pattern Recognition Letters*, vol. 22, no. 9, pp. 929–939, 2001.

[9] R. Fattal, M. Agrawala, and S. Rusinkiewicz, "Multiscale shape and detail enhancement from multi-light image collections." p. 2007.

[10] S. G. Mallat, "A theory for multiresolution signal decomposition: the wavelet representation," *Pattern Analysis and Machine Intelligence, IEEE Transactions on*, vol. 11, no. 7, pp. 674-693, 1989.

[11] M. Black, G. Sapiro, D. Marimont, and D. Heeger, "Robust anisotropic diffusion and sharpening of scalar and vector images." p. 263.

[12] S. Yang, M. Wang, L. Jiao, R. Wu, and Z. Wang, "Image fusion based on a new contourlet packet," *Information Fusion*, vol. 11, no. 2, pp. 78-84, 2010.

[13] A. L. Da Cunha, J. Zhou, and M. N. Do, "The nonsubsampled contourlet transform: theory, design, and applications," *Image Processing*,

IEEE Transactions on, vol. 15, no. 10, pp. 3089-3101, 2006.

[14] H. Li, Y. Chai, and Z. Li, "Multi-focus image fusion based on nonsubsampled contourlet transform and focused regions detection," *Optik-International Journal for Light and Electron Optics*, vol. 124, no. 1, pp. 40-51, 2013.

[15] A.-B. Petro, and C. Sbert, "Selective Contrast Adjustment by Poisson Equation," *Image Processing On Line*, vol. 2013, pp. 198-212, 2013.

[16] A. A. Goshtasby, "Fusion of multi-exposure images," *Image and Vision Computing*, vol. 23, no. 6, pp. 611-618, 2005.

[17] T. Mertens, J. Kautz, and F. Van Reeth, "Exposure fusion: A simple and practical alternative to high dynamic range photography." pp. 161-171.

[18] S. Raman, and S. Chaudhuri, "Bilateral filter based compositing for variable exposure photography," *Short Papers*, pp. 1-4, 2009.

[19] R. Shen, I. Cheng, J. Shi, and A. Basu, "Generalized random walks for fusion of multi-exposure images," *IEEE Trans Image Process*, vol. 20, no. 12, pp. 3634-46, Dec, 2011.

[20] Z. G. Li, J. H. Zheng, and S. Rahardja, "Detail-enhanced exposure fusion," *IEEE Trans Image Process*, vol. 21, no. 11, pp. 4672-6, Nov, 2012.

[21] S. J, Z. Y, Y. S, and L. X, "Exposure fusion using boosting Laplacian pyramid," *IEEE Transactions on Cybernetics*, vol. 44, 2014.

[22] O. Gallo, N. Gelfandz, W.-C. Chen, M. Tico, and K. Pulli, "Artifact-free high dynamic range imaging." pp. 1-7.

[23] J. Shen, Y. Zhao, and Y. He, "Detail-preserving exposure fusion using subband architecture," *The Visual Computer*, vol. 28, no. 5, pp. 463-473, 2012.

[24] W. Zhang, and W.-K. Cham, "Gradient-directed multiexposure composition," *Image Processing, IEEE Transactions on*, vol. 21, no. 4, pp. 2318-2323, 2012.

[25] L. Shutao, and K. Xudong, "Fast multi-exposure image fusion with median filter and recursive filter," *Consumer Electronics, IEEE Transactions on*, vol. 58, no. 2, pp. 626-632, 2012.

[26] N. Limare, J.-L. Lisani, J.-M. Morel, A. B. Petro, and C. Sbert, "Simplest color balance," *Image Processing On Line*, vol. 1, 2011.

[27] P. Getreuer, "Automatic color enhancement (ACE) and its fast implementation," *Image Processing On Line*, no. 2012, 2012.

[28] P. rez, M. Gangnet, and A. Blake, "Poisson image editing," *ACM Transactions on Graphics (TOG)*, vol. 22, no. 22, pp. 313-318, 2003.

[29] Y. Li, L. Sharan, and E. H. Adelson, "Compressing and companding high dynamic range images with subband architectures." pp. 836-844.

[30] R. Fattal, D. Lischinski, and M. Werman, "Gradient domain high dynamic range compression." pp. 249-256.

[31] Z. Li, Z. Jing, X. Yang, and S. Sun, "Color transfer based remote sensing image fusion using non-separable wavelet frame transform," *Pattern Recognition Letters*, vol. 26, no. 13, pp. 2006-2014, 2005.

[32] C. Wang, and H.-W. Shen, "Information theory in scientific visualization," *Entropy*, vol. 13, no. 1, pp. 254-273, 2011.

[33] Y. Liu, M. Liang, Y. Zhou, Y. He, Y. Hao, M. Song, C. Yu, H. Liu, Z. Liu, and T. Jiang, "Disrupted small-world networks in schizophrenia," *BRAIN*, vol. 131, no. 7, pp. 945-961, 2008.

[34] Xydeas, C.S., Petrovic, and V., "Objective image fusion performance measure," *Lron Lr*, no. 4, pp. 308-309, 2000.

[35] H. Singh, V. Kumar, and S. Bhooshan, "Anisotropic Diffusion for Details Enhancement in Multiexposure Image Fusion," *ISRN Signal Processing*, vol. 2013, 2013.